Research in Astron. Astrophys. **2009** Vol. **9** No. **5**, 520 – 528
http://www.raa-journal.org *http://www.iop.org/journals/raa*

***R**esearch in*
***A**stronomy and*
***A**strophysics*

A modified stratified model for the 3C 273 jet *

Wen-Po Liu[1,2] and Zhi-Qiang Shen[1]

[1] Key Laboratory for Research in Galaxies and Cosmology, Shanghai Astronomical Observatory, Chinese Academy of Sciences, Shanghai 200030, China; *wpliu@shao.ac.cn; zshen@shao.ac.cn*
[2] Graduate School of Chinese Academy of Sciences, Beijing 100049, China

Received 2008 July 1; accepted 2008 October 31

Abstract We present a modified stratified jet model to interpret the observed spectral energy distributions of knots in the 3C 273 jet. Based on the hypothesis of the single index of the particle energy spectrum at injection and identical emission processes among all the knots, the observed difference of spectral shape among different 3C 273 knots can be understood as a manifestation of the deviation of the equivalent Doppler factor of stratified emission regions in an individual knot from a characteristic one. The summed spectral energy distributions of all ten knots in the 3C 273 jet can be well fitted by two components: a low-energy component (radio to optical) dominated by synchrotron radiation and a high-energy component (UV, X-ray and γ-ray) dominated by inverse Compton scattering of the cosmic microwave background. This gives a consistent spectral index of $\alpha = 0.88$ ($S_\nu \propto \nu^{-\alpha}$) and a characteristic Doppler factor of 7.4. Assuming the average of the summed spectrum as the characteristic spectrum of each knot in the 3C 273 jet, we further get a distribution of Doppler factors. We discuss the possible implications of these results for the physical properties in the 3C 273 jet. Future GeV observations with *GLAST* could separate the γ-ray emission of 3C 273 from the large scale jet and the small scale jet (i.e. the core) through measuring the GeV spectrum.

Key words: galaxies: active — galaxies: individual (3C 273) — galaxies: jets — radiation mechanisms: non-thermal

1 INTRODUCTION

Being nearby ($z = 0.158$), the jet of 3C 273, which was the first quasar to be discovered (Schmidt 1963), has been studied extensively from radio (e.g., Conway et al. 1993), infrared (e.g., Jester et al. 2005; Uchiyama et al. 2006, hereafter U06; Jester et al. 2007, hereafter J07; Wen et al. 2002), optical (e.g., Jester et al. 2001, 2005; Lin 2006; Qian 2001), to X-rays (e.g., Marshall et al. 2001; Sambruna et al. 2001, hereafter S01; Jester et al. 2006, hereafter J06). A chaotic feature in the light curve of 3C 273 is also discussed by Liu (2006). A TeV flux upper limit has also been obtained by shallow *High Energy Stereoscopic System* (H.E.S.S.) observations (Aharonian et al. 2005). The $10''$-long radio jet has a knotty morphology, with the first bright knot at about $12''$–$13''$ from the central engine and increasing radio intensity toward a terminal bright hot spot about $22''$–$23''$ from the nucleus (Flatters & Conway 1985; U06).

Based on the spectral energy distributions (SEDs) of these knots and hot spots in the 3C 273 jet, many researchers have identified a two-component nature (U06; J06; S01), namely (1) the low-energy

* Supported by the National Natural Science Foundation of China.

component extending from radio to optical, and (2) the high-energy component responsible for the emission, which includes X-rays. Synchrotron emission is considered to be the dominant radiation mechanism from radio through optical bands, i.e., the low-energy component (S01; U06), but the radiation mechanism of X-ray emission is still perplexing. So far, there have been three candidates for the origin of the X-rays (S01): (a) synchrotron emission which another much more energetic population of particles emit (Röser et al. 2000; Aharonian 2002; Bai & Lee 2003; U06); (b) inverse Compton scattering of synchrotron photons from the low energy component, i.e. a Self-Synchrotron Compton (SSC) model; and (c) inverse Compton scattering of photons which are external to the jet, such as an inverse Compton scattering of photons from cosmic microwave background model (hereafter IC/CMB).

SSC emission from electrons in an equipartition magnetic field can usually account for the X-ray emission from hot spots (J07, Harris & Krawczynski 2006). However, S01 and J06 showed that the contribution from SSC X-rays in the 3C 273 jet is not significant, so we provisionally ignored the SSC effect on X-ray emission. Georganopoulos et al. (2006, hereafter G06) have presented some diagnostics (the synchrotron model needs multi-TeV electrons responsible for production of X-rays, but the IC/CMB model requires a cutoff which is lower than TeV in the SED) to distinguish the synchrotron and IC/CMB models. The γ-rays predicted by these two models can be tested through GeV and TeV observations of the 3C 273 large-scale jet. U06 described the wide radio-to-X-ray spectrum with their double power-law models (eq. (1) of U06, low-energy component with an exponential cutoff), but they required an additional assumption that the two power-law indices were different and their formula was partly ad hoc rather than derived from any clear physical insight. The double synchrotron emission model also does not clearly point out the direct connection of the two populations of source particles, and the second, the ultra-energetic particles that emit X-ray photons, calls for a radical rethink of the physics of relativistic jets driven by black holes (Urry 2006).

Among the suggested mechanisms for the high-energy component, we adopt the IC/CMB model if there is a bulk relativistic motion on kiloparsec scales (S01). Indeed, VLBI observations have detected apparent superluminal motions in the parsec-scale jet with apparent velocities ~ 6–$10\,c$ (e.g., Unwin et al. 1985). X-ray/optical emission remains asymmetric, also implying the presence of relativistic bulk motion on kiloparsec scales (S01). J06 presented deeper Chandra observations of the 3C 273 jet and found that the X-ray spectra are softer than the radio spectra in nearly all parts of the jet, ruling out the simplest one-zone beamed IC/CMB models for the X-ray emission from the entire jet. Within their two-zone jet model, they still required two different spectral indices for the radio and X-ray spectrum of each knot in the 3C 273 jet. G06 summed the fluxes of 3C 273 knots excluding the bright knots A and B as a "big knot", and they predicted the γ-ray emission of the 3C 273 large-scale jet by applying (not fitting) the IC/CMB model to the "big knot". S01 divided all the detected knots into four regions, and then fit the IC/CMB model to the wide-band SED in each of them quite well, implying the rationality of the IC/CMB model for the 3C 273 jet. Then, the question is why the IC/CMB model could fit the regions enclosing some neighboring knots but not an individual knot. S01, J06 and G06 did not explain this interesting problem. This problem may be related to the small viewing angles of knots with stratified structure (see Sect. 2). As a result, the observed spectral shape may be modulated by different beaming effects on the flux. Because S01 encloses some neighboring knots, it thus minimizes the deviation of the spectrum from that of a single component.

By now, all the fitted models on the SEDs of knots in the 3C 273 jet have assumed a single Doppler factor for emission regions in the 3C 273 knots and different spectral indices for the inner and outer knots (U06; J06; S01). Based on the analysis of Liu & Shen (2007) (hereafter LS07) of the radiation mechanism of knots in the M87 jet, the fitted energy spectral indices of the source particles along the jet were nearly constant, suggesting an identical acceleration and radiation mechanism for the source particles along the jet. We will try a different method (partly similar to S01 and G06's strategy of enclosing some neighboring knots) to investigate what resulted in the observed SEDs of knots in the 3C 273 jet.

In Section 2, we describe our model and strategy for SEDs of knots in the 3C 273 jet. In Section 3, we present and discuss the fitting results of this model to the summed SED of all the knots in the

3C 273 jet and give the distribution of the Doppler factor in the emission regions among all the knots. A summary is given in Section 4.

2 A MODIFIED STRATIFIED JET MODEL AND STRATEGY FOR ANALYZING THE SPECTRA OF KNOTS

The effect of the stratified emission along the jet and the effect of different emitting regions through the jet's cross section are common for the observed knot emission (Perlman et al. 1999; Marshall et al. 2002; Perlman & Wilson 2005; Harris & Krawczynski 2006). Based on the difference between the optical and radio polarimetric observations, Perlman et al. (1999) advanced a model of partial energy stratification. They illustrated that the optical-emitting electrons are located closer to the jet axis, while most of the radio-emitting electrons are located nearer to the jet surface. Further promoting this model, we think that even the optical- and radio-emitting electrons themselves may also be stratified through the jet's cross section, similar to a spine-sheath structure.

Advection and diffusion of the populations of particles along the jet with the decrease of the synchrotron lifetime from low energy to high energy would result in spatially stratified (LS07) and conical emission layers (regions) along the jet. Because of the cooling process, the stratified effect along the jet may be more obvious for high energy electrons. This scenario suggests that the observed differences in radiation from a knot at different frequencies are not from a simple component within the same region of that knot, but from a more complicated one whose stratified emission layers roughly correspond to different synchrotron-emitting electrons (and so to different emissions). This is more significant for a jet with a small viewing angle. If the stratified emission layers were almost independent of each other (i.e., different emission regions could have different intrinsic velocities and/or electron distributions), their Doppler factors may be different. Otherwise, the Doppler factors should be similar to each other. If we further assume that all the conical emission layers had the same intrinsic velocity but the electron distribution of each emission layer was asymmetrical with respect to the jet axis, this results in an equivalent/averaged viewing angle for each emission layer which could have two phases, i.e., near to and away from the line of sight.

The model considered here is basically composed of two components with synchrotron radiation dominating the low-energy band and the IC/CMB dominating the high-energy emission. We adopted the synchrotron model of LS07 to describe the low-energy component. In the model (eq. (3) of LS07), they considered a decay of spectral index of injection particles possibly due to the sum of the injection spectrum from different acceleration sources with synchrotron losses in the thin acceleration region, so there are two break frequencies (eq. (5) in LS07) at two sides of which the spectral index changes for the spectra of knots in the AGN jet. The IC/CMB spectrum is an identical copy of the synchrotron one. However, since the 3C 273 jet in the high-energy component was only detected from UV to X-ray, we use the power law distribution to describe the spectrum below the first break frequency which falls in the γ-ray band.

Our modified stratified jet model showed that the stratified emission layers in a knot may have different equivalent/averaged Doppler factors (i.e., Doppler factors may be roughly a function of synchrotron frequency). In particular, when the bulk velocity of advection in the 3C 273 jet approaches light speed and the equivalent/averaged viewing angle of emission layers is very small, both the Doppler factor and apparent motion of emission regions in the 3C 273 knots are sensitive to the change of velocities and equivalent viewing angles of emission layers. For synchrotron emission, the observed fluxes ($S_\nu \propto \nu^{-\alpha}$, α is the spectral index) at different frequencies are related to their Doppler factors by $S_{\nu_1}/S_{\nu_2} = (\delta_1/\delta_2)^{3+\alpha} \times (\nu_1/\nu_2)^{-\alpha}$ (Dermer 1995), and for IC/CMB emission, the relation is $S_{\nu_1}/S_{\nu_2} = (\delta_1/\delta_2)^{4+2\alpha} \times (\nu_1/\nu_2)^{-\alpha}$ (Dermer 1995). This flux ratio is very sensitive to the ratio of the Doppler factors, implying that different bulk velocities and the equivalent viewing angles (i.e., different equivalent Doppler factors) can easily cause the differences in the spectral shapes of knots in the 3C 273 jet.

Because we do not know the real Doppler factor distribution for emission regions along the 3C 273 jet, in our analysis, we assumed that the deviations of the observed spectral shape for emission regions

along the 3C 273 jet is somehow symmetric with a hypothetical characteristic one, and so we obtain such a characteristic one by averaging SEDs of all the knots in the 3C 273 jet. This is justified by the reasonable fitting results of the spectral shapes and Doppler factors (see Sect. 3). As such, the increasing lower-energy emissions and decreasing high-energy emissions with increasing separation from the nucleus (U06) can be ascribed to the deviation of the Doppler factor of each knot from the characteristic one in the 3C 273 jet. The detailed distribution of magnetic field and electron velocity directions may also affect the observed spectral shape of knots, but for simplicity, we do not consider this case. The SED of an individual knot in the M87 Jet (with a larger viewing angle than the 3C 273 Jet) could be fitted by a continuous injection (CI) synchrotron with a break power law (LS07), but this is not the case in 3C 273. By assuming the effects of intrinsic conditions (such as volume, kinetic age, electron normalization constant and distribution of magnetic field and electron velocity directions etc.) of jets in M87 and 3C 273 are similar to the observed synchrotron spectrum of an individual knot, we think that the deviation of the observed spectral shape of an individual knot in the 3C 273 jet from the CI synchrotron one is caused by some external effects likely related to the different viewing angles. According to this viewpoint, the spectrum of every knot in the 3C 273 jet is modulated by different equivalent Doppler factors in the stratified emission layers, resulting in models with a single Doppler factor being ineffective for knots (such as IC/CMB in J06). However, the summed spectrum of all the knots may minimize such an effect (partly similar to S01's strategy of enclosing some neighboring knots) and therefore can be treated as a representative SED of a "big knot" with a single Doppler factor and spectral index. In the following, unlike G06's illustration (not fitting) of a "big knot" (excluding the bright knots A and B), we will first get a quantitative description of the characteristic spectrum of our "big knot" (including all the 3C 273 knots) by means of a two-component fitting. Then, we will discuss the deviation of Doppler factors in each knot by comparing their SEDs with this characteristic one.

3 FITTING RESULTS AND DISCUSSION

In Table 1, the data for the knots (except knot H1) were from J07. For knot H1, the *VLA* and *HST* data are taken from Jester et al. (2005), and the *Spitzer* data from U06. It was not detected by *Chandra* in X-ray or the other three *HST* bands. The error bars for the radio, optical and X-ray data were estimated separately by increasing $5-20$ times the r.m.s noise in J07, within the range of the flux errors (1%–5% in all cases for both the radio and optical measurements, and less than 10% for most of the X-ray measurements, U06). A formal fractional uncertainty of 10% is assigned to the *Spitzer* data to account for systematic errors of 2%–10% (U06). By summing the flux densities and error bars of all the knots in the 3C 273 jet, we obtained the SED for the $10''$-long jet (as the "big knot"). We then performed the weighted least-squares method to fit the two-component model to this SED.

Before fitting, we need to divide the available 10 data points from radio to X-rays into two groups to match the corresponding low- and high-energy components. By examining the shape of the SED in Figure 1, it is likely that the cutoff frequency between the two components is around 1.0×10^{15} Hz. This makes it difficult to decide the dominant mechanism for the *HST* measurement at 1.0×10^{15} Hz. Therefore, we first did two fits of the low-energy synchrotron emission to the data sets with and without the 1.0×10^{15} Hz measurement, respectively. We found that fitting with this *HST* data point gave 3–4 times larger reduced chi-squares (χ^2_ν). Thus, we chose to interpret the emission at 1.0×10^{15} Hz as being dominated by the IC/CMB. So, the cutoff frequency between the upper limit frequency of the low-energy component and the lower limit frequency of the high-energy component is within 4.85×10^{14} to 1.00×10^{15} Hz.

Once we have fixed such a cutoff frequency, we can perform an independent spectral fitting to both low- and high-energy components as described in Section 2. In practice, we fit the synchrotron model (eq. (5) of LS07, with 4 parameters) to the 7 data points at frequencies lower than 1.0×10^{15} Hz. In this process, a power-law form is chosen near the break frequencies because we only need to be concerned with the trend of the break frequencies. There are two break frequencies in our model, but we do not know exactly where they are when we fit to the chosen data in Figure 1. So, we first arbitrarily divide observational data into three groups to perform the fitting and calculate the corresponding χ^2_ν

Table 1 Flux Densities of Knots in 3C 273 Jet

	Flux Density[1]					
Frequency (Hz)	A	B1	B2	B3	C1	C2
VLA[2] (mJy):						
8.33×10^9	90.5 ± 1.30	69.2 ± 1.07	105 ± 1.43	50.8 ± 1.01	101 ± 1.56	205 ± 2.47
1.5×10^{10}	58.9 ± 0.66	41.9 ± 0.53	69 ± 0.77	34.8 ± 0.59	67 ± 0.90	134 ± 1.56
2.25×10^{10}	38.5 ± 0.49	30.6 ± 0.42	50.8 ± 0.60	23.6 ± 0.43	48.8 ± 0.69	97.1 ± 1.12
Sptizer (μJy):						
5.23×10^{13}	45 ± 10	35 ± 12	36.2 ± 8.1	12.8 ± 2.9	98 ± 11	89 ± 12
8.45×10^{13}	27 ± 2.7[3]	15 ± 2.6	28.8 ± 2.88[3]	10.2 ± 1.02[3]	36 ± 3.6[3]	46 ± 4.6[3]
HST[2] (μJy):						
1.87×10^{14}	11.3 ± 0.48	4.9 ± 0.17	10.2 ± 0.20	4.84 ± 0.12	10.8 ± 0.17	18.1 ± 0.20
4.85×10^{14}	4.93 ± 0.12	1.83 ± 0.082	3.86 ± 0.098	1.37 ± 0.059	2.93 ± 0.079	3.93 ± 0.09
1.00×10^{15}	3.2 ± 0.17	0.973 ± 0.06	1.88 ± 0.07	0.507 ± 0.04	1.16 ± 0.06	1.28 ± 0.06
1.86×10^{15}	2.03 ± 0.11	0.626 ± 0.037	1.47 ± 0.079	0.439 ± 0.028	0.657 ± 0.039	0.723 ± 0.042
Chandra[2] (nJy):						
2.42×10^{17}	46.5 ± 2.70	10.9 ± 1.25	20 ± 1.65	3.41 ± 0.70	4.85 ± 0.80	6.25 ± 0.90

	Flux Density[1]				
Frequency (Hz)	D1	D2H3	H2	H1	Sum[4]
VLA[2] (mJy):					
8.33×10^9	283 ± 3.9	836 ± 8.84	1330 ± 16.90	571.9 ± 7.27	3400.5 ± 45.75
1.5×10^{10}	182 ± 2.34	516 ± 5.33	782 ± 9.62	398.4 ± 4.90	2085.6 ± 27.20
2.25×10^{10}	131 ± 1.69	357 ± 3.64	520 ± 6.24	208.0 ± 2.50	1427.4 ± 17.82
Sptizer (μJy):					
5.23×10^{13}	154 ± 15.4[3]	161 ± 16.1[3]	87 ± 12	28 ± 11	746 ± 110.5
8.45×10^{13}	80 ± 8[3]	140 ± 14[3]	41 ± 4.1[3]	10 ± 2.6	434 ± 46.1
HST[2] (μJy):					
1.87×10^{14}	21.7 ± 0.19	40 ± 0.28	6.97 ± 0.19	2.04 ± 0.06	130.31 ± 2.06
4.85×10^{14}	3.56 ± 0.08	7.68 ± 0.1	1.29 ± 0.09	$\cdots$	31.38 ± 0.72
1.00×10^{15}	1.09 ± 0.05	2.54 ± 0.07	0.459 ± 0.07	$\cdots$	13.09 ± 0.65
1.86×10^{15}	0.679 ± 0.04	1.39 ± 0.075	0.288 ± 0.02	$\cdots$	8.302 ± 0.47
Chandra[2] (nJy):					
2.42×10^{17}	5.16 ± 0.85	7.82 ± 1.00	1.3 ± 0.45	$\cdots$	106.19 ± 10.30

[1]The data of the knots except knot H1 were from J07. The *VLA* and *HST* data of knot H1 were from Jester et al. (2005), but the *Spitzer* data of knot H1 were from U06. [2]The error bars for the *VLA*, *HST* (except for 1.86×10^{15} Hz) and *Chandra* data were estimated separately by increasing $5 - 20$ times the r.m.s noise in these data from J07. [3]A formal fractional uncertainty of 10% is assigned to the *Spitzer* data to account for the systematic errors of 2%–10% (U06). [4]The sum of the flux densities and error bars for the knots in the 3C 273 jet.

by changing the division. All the possible combinations are tried before we obtain the best fit with a minimal χ^2_ν among them. For the high-energy component fit to the remaining 3 high frequency data points, only a power law (with 2 parameters) is needed. In Table 2 are shown the fitting results. The SED for the "big knot" in the 3C 273 jet and the best fits are plotted in Figure 1. Therefore, both the high and low-energy components are independently described by our model. The fitted spectral indices of the low-energy (0.87 ± 0.02) and high-energy (0.88 ± 0.02) components are very consistent with each other, supporting the IC/CMB nature of the high-energy component. The corresponding value of the particle spectral index ($p = 2\alpha + 1$) of 2.76 is also in the characteristic range ($2 < p < 3.5$, Blumenthal & Gould 1970).

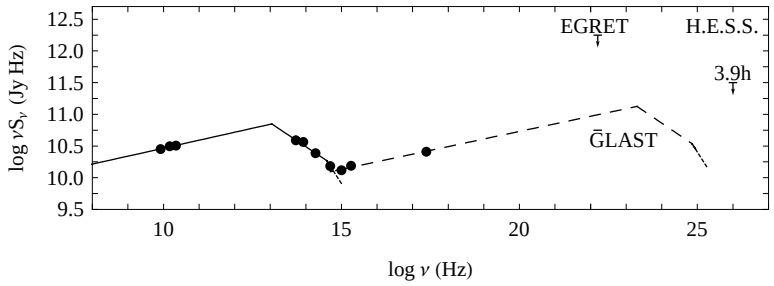

Fig. 1 SED for the summed knots in the 3C 273 jet from radio through to X-ray wavelengths. The solid line displays the model fit to the low-energy component, and the dashed line to the high-energy component. The dotted lines show the possible cutoff frequency band for the two components. The error bars of most measurements are too small to be seen here. The EGRET upper limit and the *GLAST* sensitivity limit are also shown, as well as a TeV flux upper limit from shallow H.E.S.S. observations (Aharonian et al. 2005).

Table 2 Parameters of Model Fits from Radio to X-ray Data

Parameters	Model	α	χ^2_ν	$\nu_{\rm peak}$(Hz)	δ
Low-energy Component	Synchrotron	0.87 ± 0.02	1.18	1.10×10^{13}	7.4 ± 0.5
High-energy Component	IC/CMB	0.88 ± 0.02	1.51	2.00×10^{23}	$\cdots$

Col. (1): Component designation. Col. (2): Model designation. Col. (3): Spectral index. Col. (4): Reduced chi square. Col. (5): Peak frequency, note that the peak frequency for high-energy component is a derived parameter. Col. (6): Characteristic Doppler factor.

The fitted synchrotron component has a total power of $L_{\rm s} \approx 5.2 \times 10^{41}$ erg s^{-1}, which is actually dominated by the emission around the peak frequency, i.e., $L_{\rm s} \approx 4\pi D_{\rm L}^2[\nu_{\rm s,p} S(\nu_{\rm s,p})/(1-\alpha) + \nu_{\rm s,p} S(\nu_{\rm s,p})/(\alpha - 0.5)]$, here $S(\nu_{\rm s,p})$ is the flux density at the peak frequency $\nu_{\rm s,p} \approx 1.10 \times 10^{13}$ Hz (see Table 2), and a luminosity distance of $D_{\rm L} = 749$ Mpc is adopted. Accordingly, we can estimate the luminosity of IC/CMB emission, which is also dominated by the emission around its peak frequency $\nu_{\rm c,p}$. Thus, we can get a ratio between the IC/CMB luminosity and synchrotron luminosity as follows

$$\frac{L_{\rm c}}{L_{\rm s}} = \frac{\nu_{\rm c,p}\ S(\nu_{\rm c,p})}{\nu_{\rm s,p}\ S(\nu_{\rm s,p})}\,. \tag{1}$$

According to Geoganopoulos et al. (2006), this luminosity ratio is related to the Doppler factor as

$$\frac{L_{\rm c}}{L_{\rm s}} = 6.25 \times 10^{-4}\ \delta^4\,, \tag{2}$$

and the two peak frequencies ($\nu_{\rm c,p}$ and $\nu_{\rm s,p}$) are related by the expression

$$\nu_{\rm c,p} = 3.3 \times 10^8\ \delta^2\ \nu_{\rm s,p}\,. \tag{3}$$

It should be mentioned that in getting Equations (2) and (3), an equipartition magnetic field $B\delta \approx 2 \times 10^{-4}$G (Jester et al. 2005) is used. These equations require that the electrons which emit synchrotron photons (i.e., the first component of the SED) upscatter the CMB, and the resulting IC/CMB SED (i.e., the second component) is an exact copy of the synchrotron one (G06). This is consistent with our model for the large scale jet as a "big knot" (our synchrotron model is somewhat different from the one of G06, but this does not influence the validity of the equations in the letter), so these equations are still valid in our model. Finally, from our fitting results, we can obtain the characteristic Doppler factor $\delta \approx 7.4$ which

agrees with the requirement of FSRQ's Doppler factor (> 6.45, Cao & Bai 2008) well. This may verify the Uniform Scheme for quasars (Urry & Padovani 1995). The frequency shift between IC/CMB and synchrotron emissions is $\nu_{\rm c}/\nu_{\rm s} \sim 1.81\times10^{10}$, here $\nu_{\rm c}$ and $\nu_{\rm s}$ are the observed IC/CMB and synchrotron frequencies, respectively. Then, we could estimate the equipartition magnetic field $B = 27\mu$G and a synchrotron lifetime of ~ 4000 yr, (eq. (4) of U06) of the "big knot" which is smaller than the source kinetic age ($10^5 \sim 10^7$ yr, U06). This means that a continuous injection of electrons is responsible for the SED of the 3C 273 jet. The peak frequency of the high-energy component is at 2.00×10^{23} Hz $\sim$1 GeV (see Table 2), around the working band of the *Energetic Gamma-Ray Experiment Telescope* (EGRET) on the *Compton Gamma-Ray Observatory* (CGRO) and the current *Gamma-Ray Large Area Space Telescope* (*GLAST*). The model predicted γ-ray flux was at least 10 times lower than the EGRET upper limit (von Montigny et al. 1997; Geoganopoulos et al. 2006), but should be detectable by *GLAST* (see Fig. 1). Although *GLAST* (e.g., the expected 68% containment angular resolution of *GLAST* LAT is 0.15° (on-axis) for photons above 10 GeV, *GLAST* website) could not separate the γ-ray emission from the large scale jet and the core, by measuring the SED of the GeV energies, we still could identify the origin of the GeV emission (the large scale jet or the small scale jet, i.e. the core). The high-frequency cutoff of the second component appears at the band between 8.8×10^{24} and 1.8×10^{25} Hz (lower than the TeV band), which is consistent with the non-detection by shallow H.E.S.S. observations (Aharonian et al. 2005) as shown in Figure 1.

Based on the model described in Section 2, the observed spectrum of individual knots in the 3C 273 jet may result from the stratified emission layers in which the Doppler factors deviate from the characteristic one. So, unless the deviation effect of Doppler factors in the observed spectrum of each knot is removed, otherwise those fitted spectral indices for radio and X-ray bands of each knot (Jester et al. 2005; J06; J07) may not really reflect the intrinsic and characteristic spectral shape of the 3C273 jet. Here, for comparison, we take the average of the summed spectrum as the characteristic spectrum of each knot in the 3C 273 jet. Then, through the ratio of the observed to average flux densities of each knot and the aforementioned formula in Section 2, we could derive a distribution of the Doppler factor in the spatially stratified emission regions of the 3C 273 knots (Fig. 2). The error bars of derived Doppler factors could be evaluated from the ones for observed flux and the characteristic Doppler factor, and are also plotted in Figure 2. Furthermore, by assuming a constant bulk velocity of the emission layers along the jet (we chose the bulk velocity that satisfies the average apparent velocity 8c and the characteristic Doppler factor 7.4), we can obtain their equivalent viewing angle distribution of 5° to 11° with an average of 7.7° from their Doppler factor distribution. The averaged viewing angle distribution of emission layers in each knot could be explained by the combination of different equivalent viewing angle phases (i.e., near to and away from the viewing line) of different emission layers in each knot. As expected, the trend of the Doppler factor distribution is almost opposite to the equivalent viewing angle distribution.

The derived Doppler factors at radio frequency ($\sim 10^{10}$ Hz) in each knot are almost the same (Fig. 2). This indicated that these radio-emitting electron regions are not independent. The Doppler factors at optical emission around 10^{14} Hz in 3C 273 knots are distinctly different from each other (Fig. 2), implying that these optical-emitting electron layers are likely to be independent. As these optical data are present up to the break frequency of 3C 273 knots, and the cooling effect of optical-emitting electrons is more severe than radio-emitting electrons, then the stratified effect of these optical-emitting electrons is also more obvious than that of radio-emitting electrons.

Based on our fits, the observed spectral shape of the X-ray spectrum ($\sim 10^{18}$ Hz) in the high-energy component actually reflects the spectrum of particles that emit photons at a frequency below 5.51×10^7 Hz. Although the low-frequency emissions may be severely absorbed, the particles in the emission regions could still scatter off the CMB photons to the X-ray band. So, the Doppler factors of the high-energy component actually represent the ones from the low-energy component. Based on our modified stratified jet model as described in Section 2, those below 5.51×10^7 Hz radio-emitting electron regions are mainly located nearer to the jet surface, and are almost independent of the $\sim 10^{10}$ Hz radio-emitting electron regions. Therefore, the Doppler factors of these two bands are also different. For the inner knots (such as knots A, B1, B2 and B3 in Fig. 2), the equivalent Doppler factors of the emission

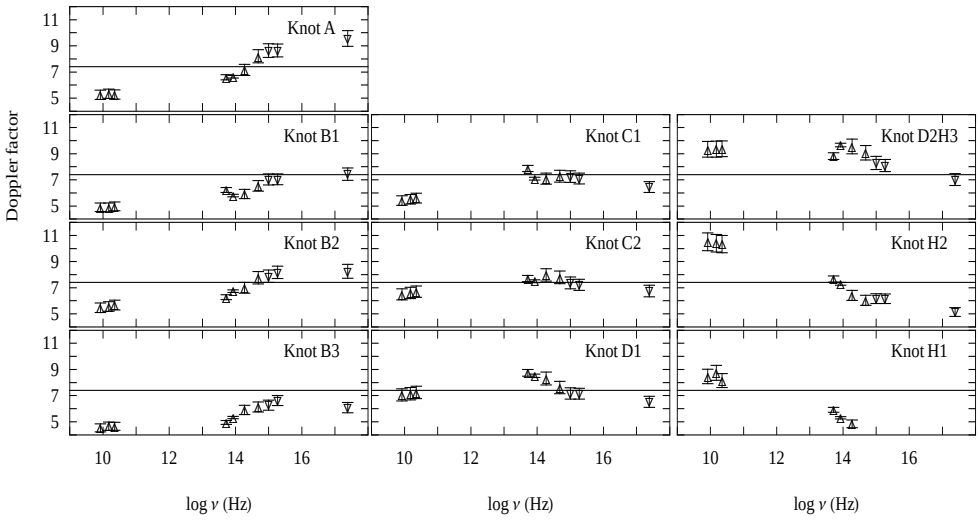

Fig. 2 Distribution of the Doppler factor of each knot as a function of the observing frequency. The low-frequency component from radio to optical is plotted as empty-up-triangles and the high-frequency component as filled-down-triangles. The error bars are also plotted in the data. The left, middle and right panels show inner, intermediate and outer knots in the 3C 273 jet respectively, with a characteristic Doppler factor of 7.4 in the 3C 273 jet indicated by a straight line.

regions where the particles scatter the CMB photons to the X-ray band are larger than the ones of the emission regions that mainly emit photons between 10^{10} and 10^{15} Hz (see Fig. 2). This explains why the observed SEDs of the inner knots are dominated by the high-energy component (see fig. 2 of J07 and fig. 5 of U06). For the outer knots (such as knots D2H3, H2 and H1 in Fig. 2), the Doppler factors of the emission regions where the particles scatter the CMB photons to the X-ray band overall are smaller than the ones of emission regions that mainly emit photons between 10^{10} and 10^{15} Hz. This results in the observed SEDs of the outer knots being dominated by the low-energy component. The intermediate knots (such as knots C1, C2 and D1 in Fig. 2) show almost identical Doppler factors among all the observed emission regions.

4 CONCLUSIONS

Based on the hypothesis of the same intrinsic SED for all the knots in the 3C 273 jet, the differences in their spectral shape are interpreted as a result of the differences of the equivalent Doppler factors of our modified stratified emission layers. Furthermore, if we assume a constant bulk velocity of the emission regions along the jet, the Doppler factor distribution could be due to the equivalent/averaged viewing angle distribution for the spatially stratified emission layers of the knots in the 3C 273 jet. Our fitting to the summed spectrum supports the notion that high energy X-ray emission is dominated by inverse Compton scattering of the cosmic microwave background. The predicted γ-ray spectrum of the large-scale jet in 3C 273 could be further tested by measuring its GeV spectrum from *GLAST* observations. It should be noted that our model needs the stratified synchrotron-emitting electrons, which should be verified by further multi-band observations.

Acknowledgements We thank S. Jester for helpful communications and for supplying his data to us for reference. Many thanks are due to the referee for constructive comments. We also thank the ChJAA's (now called RAA) editor Jingzhi Zhao for her conscientious work. This work has been partially supported by the National Natural Science Foundation of China (grants 10573029, 10625314, 10633010

and 10821302) and the Knowledge Innovation Program of the Chinese Academy of Sciences (Grant No. KJCX2-YW-T03), and sponsored by the Program of Shanghai Subject Chief Scientist (06XD14024) and the National Key Basic Research Development Program of China (No. 2007CB815405).

References

Aharonian, F., et al. 2002, MNRAS, 332, 215
Aharonian, F., et al. 2005, A&A, 441, 465
Bai, J. M., & Lee, M. G. 2003, ApJ, 585, L113
Blumenthal, G. R., & Gould, R. J. 1970, Rev. Mod. Phys., 42, 237
Cao, X., & Bai, J. M. 2008, ApJ, 673, L131
Conway, R, G., Garrington, S. T., Perley, R. A., & Biretta, J. A. 1993, A&A, 267, 347
Dermer, C. D. 1995, ApJ, 446, L63
Flatters, C., & Conway, R. G. 1985, Nature, 314, 425
Georganopoulos, M., Perlman, E. S., Kazanas, D., & McEnery, J. 2006, ApJ, 653, L5 (G06)
GLAST website, *http://fermi.gsfc.nasa.gov/*
Harris, D. E., & Krawczynski, H. 2006, ARA&A, 44, 463
Jester, S., Harris, D. E., Marshall, H. L., & Meisenheimer, K. 2006, ApJ, 648, 900 (J06)
Jester, S., Röser, H.-J., Meisenheimer, K., & Perley, R. A. 2005, A&A, 431, 477
Jester, S., Röser, H.-J., Meisenheimer, K., Perley, R. A., & Conway, R. G. 2001, A&A, 373, 447
Jester, S., et al. 2007, MNRAS, 380, 828 (J07)
Kardashev, N. S. 1962, Soviet Astron., 6, 317
Liu, L. 2006, ChJAA (Chin. J. Astron. Astrophys.), 6, 663
Lin, R.-G. 2001, ChJAA (Chin. J. Astron. Astrophys.), 1, 245
Liu, W.-P., & Shen, Z.-Q. 2007, ApJ, 668, L23 (LS07)
Marshall, H. L., et al. 2001, ApJ, 549, L167
Marshall, H. L., et al. 2002, ApJ, 564, 683
Perlman, E. S., Biretta, J. A., Zhou, F., Sparks, W. B., & Macchetto, F. D. 1999, AJ, 117, 2185
Perlman, E. S., & Wilson, A. S. 2005, ApJ, 627, 140
Qian, S.-J., Zhang, X.-Z., Krichbaum, T.-P., et al. 2001, ChJAA (Chin. J. Astron. Astrophys.), 1, 236
Röser, H.-J, Meisenheimer, K., Neumann, M., Conway, R. G., & Perley, R. A. 2000, A&A, 360, 99
Sambruna, R. M., et al. 2001, ApJ, 549, L161 (S01)
Schimidt, M. 1963, Nature, 197, 1040
Uchiyama, Y., et al. 2006, ApJ, 648, 910 (U06)
Unwin, S. C., et al. 1985, ApJ, 289, 109
Urry, C. M. 2006, *http://www.physorg.com/news70016047.html*
Urry, C. M., & Padovani, P. 1995, PASP, 107, 803
von Montigny, C., Aller, H. D., & Aller, M. F. 1997, ApJ, 483, 161
Wen, S.-L., Peng, Z.-M., Fan, J.-H., & Xie, G.-Z. 2002, ChA&A, 26, 398